Supplementary Materials

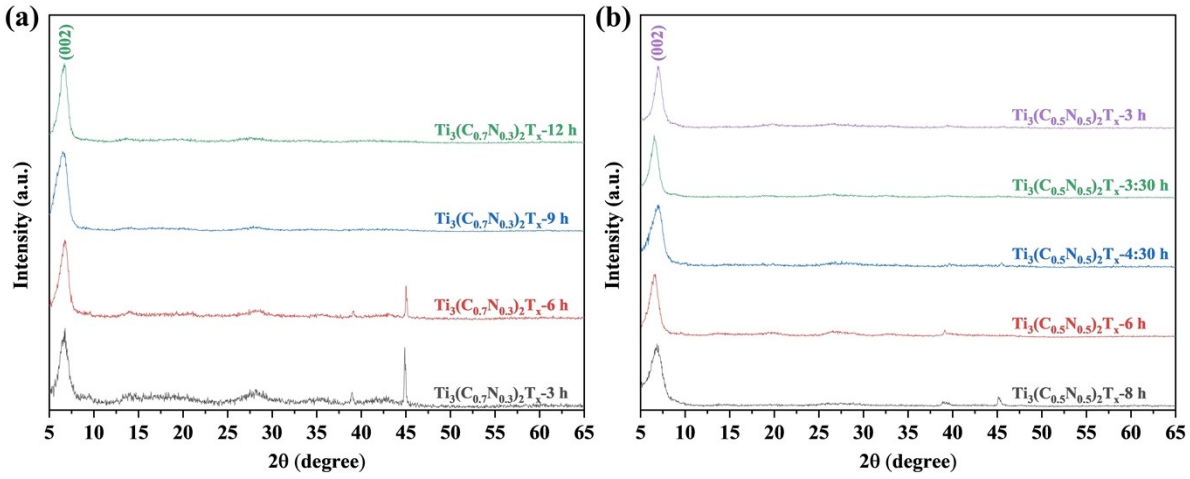

Fig. S1 XRD patterns of MXene nanosheets synthesized under different etching conditions. (a) $Ti_3Al(C_{0.7}N_{0.3})_2$ MAX phase etched at a MAX:HCl:LiF ratio of 1 g : 60 mL : 1.89 g at 40 °C for 3, 6, 9, and 12 h. (b) $Ti_3Al(C_{0.5}N_{0.5})_2$ MAX phase etched under the same concentration ratio and temperature for 8, 6, 4 : 30, 3 : 30, and 3 h. After etching and drying, all samples were analyzed to assess phase purity and identify possible impurities.

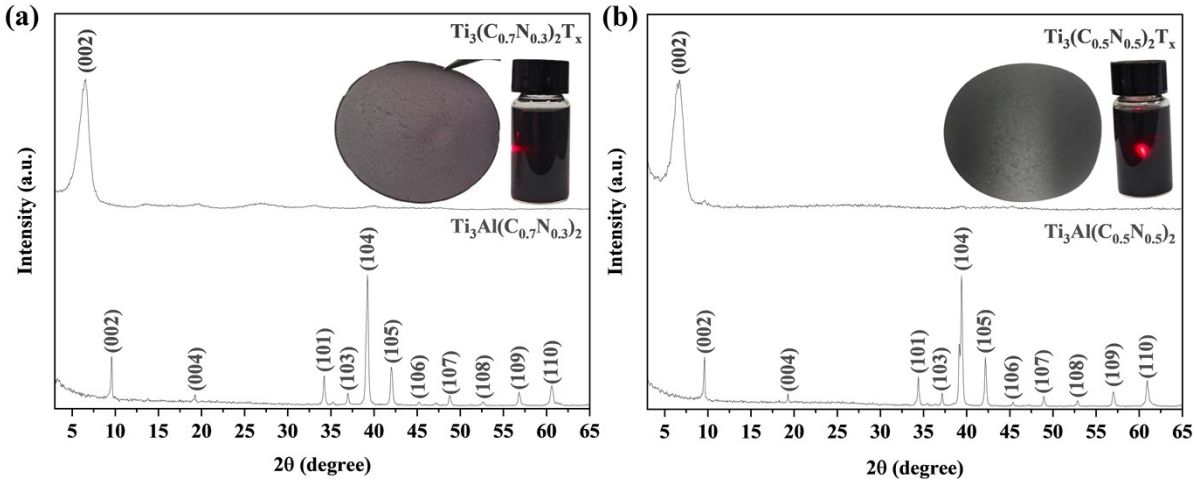

Fig. S2 XRD patterns of (a) $Ti_3Al(C_{0.7}N_{0.3})_2$ powder and $Ti_3(C_{0.7}N_{0.3})_2T_x$ MXene film after 12 h etching, along with the observed Tyndall effect and (b) $Ti_3Al(C_{0.5}N_{0.5})_2$ powder and

$Ti_3(C_{0.5}N_{0.5})_2T_x$ MXene film after 3 h etching, along with the observed Tyndall effect.

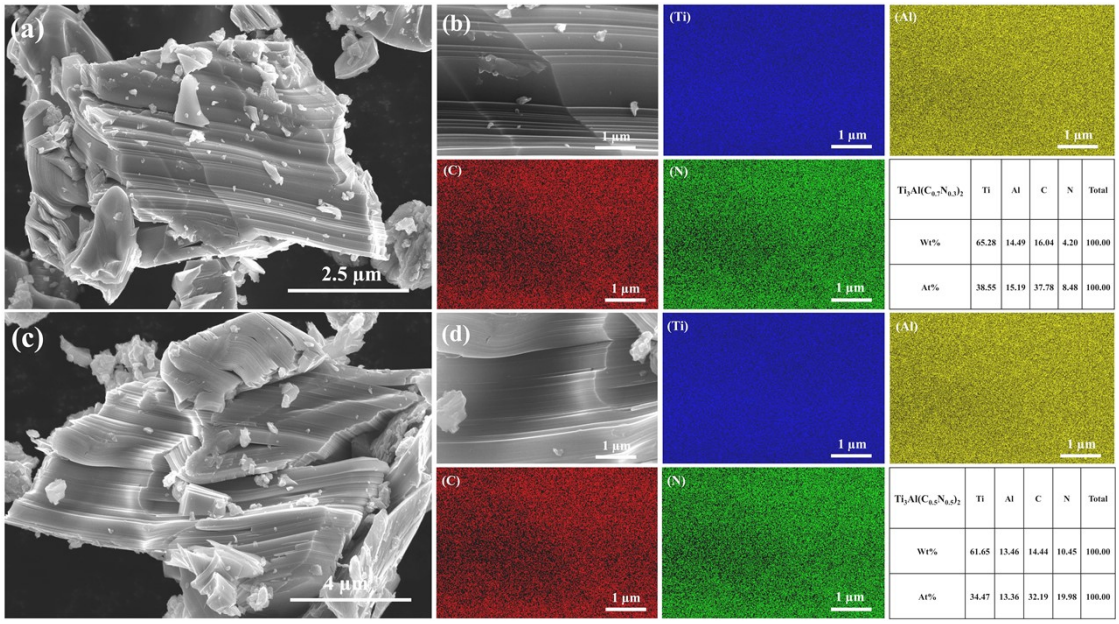

$Ti_3Al(C_{0.7}N_{0.3})_2$	Ti	Al	C	N	Total
Wt%	65.28	14.49	16.04	4.20	100.00
At%	38.55	15.19	37.78	8.48	100.00

$Ti_3Al(C_{0.5}N_{0.5})_2$	Ti	Al	C	N	Total
Wt%	61.65	13.46	14.44	10.45	100.00
At%	34.47	13.36	32.19	19.98	100.00

Fig. S3 FE-SEM images and corresponding elemental mapping of (a, b) $Ti_3Al(C_{0.7}N_{0.3})_2$ MAX phase powder and (c, d) $Ti_3Al(C_{0.5}N_{0.5})_2$ MAX phase powder.

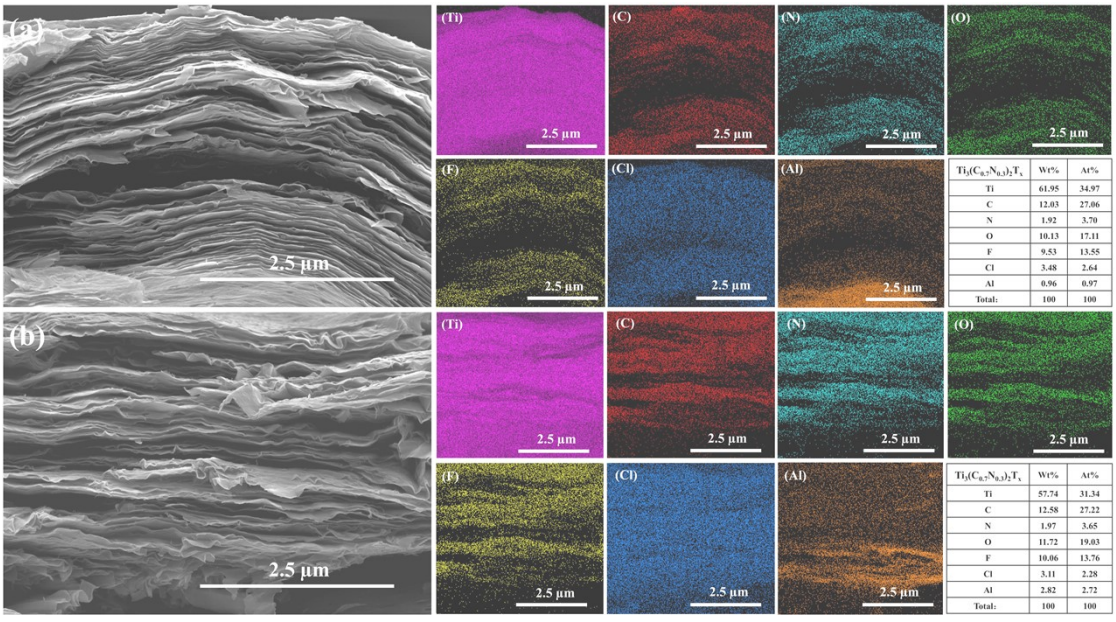

$Ti_3(C_{0.7}N_{0.3})_2T_x$	Wt%	At%
Ti	61.95	34.97
C	12.03	27.06
N	1.92	3.70
O	10.13	17.11
F	9.53	13.55
Cl	3.48	2.64
Al	0.96	0.97
Total:	100	100

$Ti_3(C_{0.7}N_{0.3})_2T_x$	Wt%	At%
Ti	57.74	31.34
C	12.58	27.22
N	1.97	3.65
O	11.72	19.03
F	10.06	13.76
Cl	3.11	2.28
Al	2.82	2.72
Total:	100	100

Fig. S4 Elemental mapping of $Ti_3(C_{0.7}N_{0.3})_2T_x$ MXene films etched for (a) 12 h and (b) 9 h.

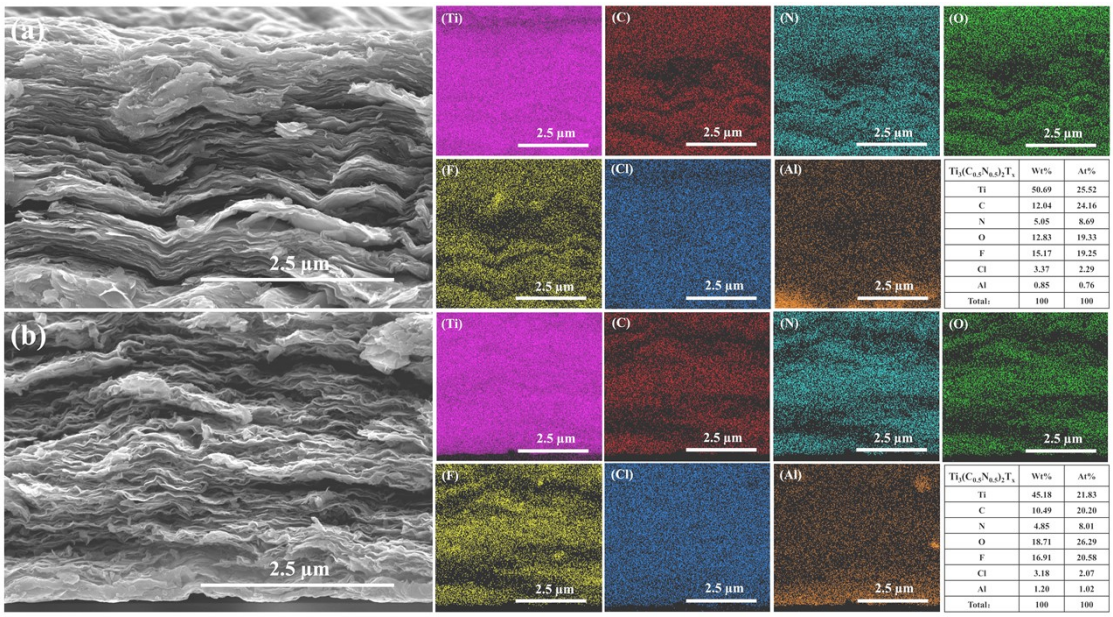

Fig. S5 Elemental mapping of $Ti_3(C_{0.5}N_{0.5})_2T_x$ MXene films etched for (a) 3 h and (b) 3:30 h.

(Fig. S3) illustrates the images and elemental mapping of $Ti_3Al(C_{0.7}N_{0.3})_2$ and $Ti_3Al(C_{0.5}N_{0.5})_2$ MAX phase obtained through EDS. The MAX phase samples exhibit a homogeneous distribution of all constituent elements across the surface of the $Ti_3Al(C_{0.7}N_{0.3})_2$ and $Ti_3Al(C_{0.5}N_{0.5})_2$ MAX phase particles. (Fig. S4) illustrates the corresponding elemental mapping of $Ti_3(C_{0.7}N_{0.3})_2T_x$ MXene films etched for 12 and 9 h, respectively. (Fig. S5) illustrates the corresponding elemental mapping of $Ti_3(C_{0.5}N_{0.5})_2T_x$ MXene films etched for 3 and 3:30 h, respectively. Both optimized MXene films etched for 12 and 3 h exhibit a homogeneous distribution of all constituent elements across the MXene surface and show the

highest electrical conductivity among the all MXenes samples. The significantly reduced aluminum concentration indicates efficient removal of the Al layer during etching. Furthermore, the presence of surface in the –O, –F, and –Cl from the etching reactions involving HCl and LiF. The atomic percentages of Ti, Al, C, and N in the $Ti_3Al(C_{0.7}N_{0.3})_2$ MAX phase powder were determined to be 38.55, 15.19, 37.78, and 8.48%, respectively (Fig. S3a). In comparison, the corresponding atomic percentages in the $Ti_3Al(C_{0.5}N_{0.5})_2$ MAX phase powder were 34.47, 13.36, 32.19, and 19.98%, respectively (Fig. S3b). The higher nitrogen content in the $Ti_3Al(C_{0.5}N_{0.5})_2$ phase reflects the intended compositional adjustment and confirms successful nitrogen incorporation into the MAX structure.[1] The atomic percentages of Ti, C, N, O, F, Cl, and Al in the $Ti_3(C_{0.7}N_{0.3})_2T_x$ MXene film etched for 12 h were determined to be 34.97, 27.06, 3.70, 17.11, 13.55, 2.64, and 0.97 at.% (Fig. S4a). In comparison, the corresponding atomic percentages in the $Ti_3(C_{0.5}N_{0.5})_2T_x$ MXene film etched for 3 h were 25.52, 24.16, 8.69, 19.33, 19.25, 2.29, and 0.76 at.% (Fig. S5a). The higher nitrogen and fluorine contents in $Ti_3(C_{0.7}N_{0.3})_2T_x$ etched for 12 h and $Ti_3(C_{0.5}N_{0.5})_2T_x$ etched for 3 h, suggests more effective surface functionalization during etching, while the reduced titanium and carbon content reflects the changes in stoichiometry and surface termination introduced by the different etching durations and compositions.[2, 3]

Specifically, systematic optimization studies supported by XRD, EDS, and elemental mapping analyses. For $Ti_3Al(C_{0.7}N_{0.3})_2$, shorter etching times (e.g., 9 h) resulted in incomplete removal of the Al layer, as evidenced by residual MAX phase peaks in XRD and non-uniform elemental distribution in EDS mapping. In contrast, 12 h etching led to complete suppression

of MAX phase reflections, a characteristic shift of the (002) peak to lower angles, and homogeneous elemental distribution, confirming successful MXene formation.

For $Ti_3Al(C_{0.5}N_{0.5})_2$, complete phase transformation was achieved within 3 h due to relatively faster etching kinetics associated with higher nitrogen content. Prolonged etching (e.g., 3.5 h) did not further improve phase purity and showed indications of structural degradation. Corresponding EDS and elemental mapping results confirmed efficient Al removal and uniform composition at 3 h. Therefore, the selected etching times represent optimized conditions for achieving complete etching while preserving structural integrity.

Table. S1 Electrical conductivity, Thickness, Density and electromagnetic interference shielding performance of $Ti_3(C_{1-y}N_y)_2T_x$ $(y = 0.3, 0.5)$ MXenes, C:P, and M_x/C:P composite films.

Sample	Electrical conductivity σ (S m^{-1})	Thickness (µm)	Theoretical Density (g cm^{-3})	Experimental Density (g cm^{-3})	Porosity %	SE (dB)	SSE/t (dB cm^2 g^{-1})
$Ti_3(C_{0.7}N_{0.3})_2T_x$	295148.70 ± 3200	5	3.80	2.79	26.6	55.72	39942.65
$Ti_3(C_{0.5}N_{0.5})_2T_x$	233495.40 ± 2700	5	3.60	2.43	32.5	48.22	39687.24
C:P	26112.80 ± 629	13	1.88	1.06	43.60	35.37	25667.63
$M_{0.7}$/C:P10	90803.76 ± 611	9	3.62	2.15	40.58	42.18	30565.22
$M_{0.7}$/C:P20	76087.26 ± 531	9	3.43	2.03	40.94	45.03	33281.59
$M_{0.7}$/C:P30	57476.72 ± 512	10	3.25	1.87	42.57	36.12	27572.52
$M_{0.7}$/C:P40	45969.40 ± 488	11	3.07	1.71	44.38	34.65	26923.07
$M_{0.5}$/C:P10	78804.69 ± 587	9	3.43	1.98	42.42	39.10	27096.33
$M_{0.5}$/C:P20	64707.66 ± 523	10	3.27	1.85	43.55	41.93	29362.74
$M_{0.5}$/C:P30	48388.85 ± 478	10	3.11	1.71	45.12	35.04	25082.32
$M_{0.5}$/C:P40	40412.66 ± 411	11	2.95	1.59	46.18	32.37	23456.52

SE: shielding effectiveness; SSE/t: specific shielding effectiveness.

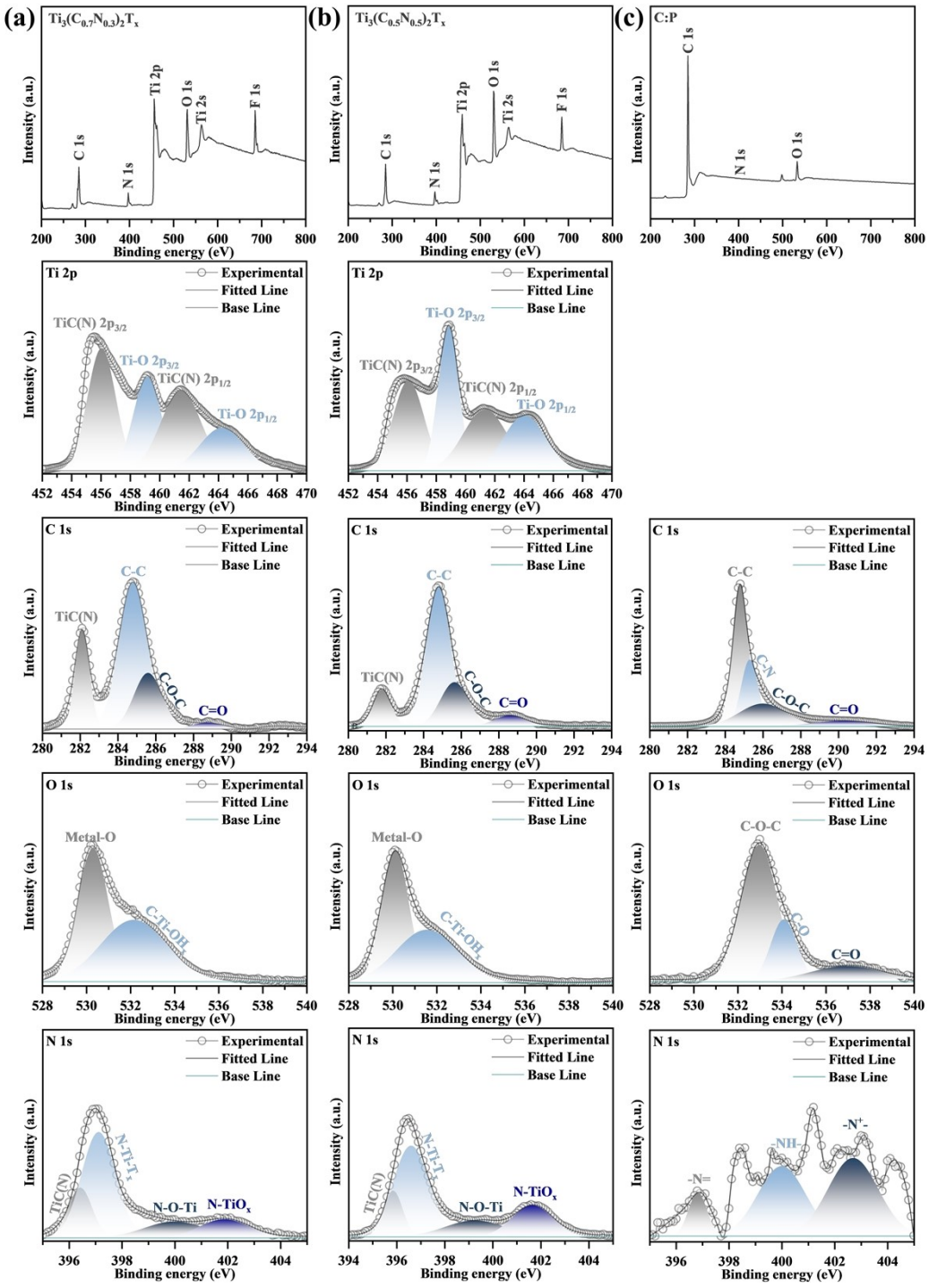

Fig. S6 XPS spectra of full-range spectrum and high-resolution spectra of (a, b) Ti, C, O, and N for $Ti_3(C_{1-y}N_y)_2T_x$ $(y = 0.3, 0.5)$ MXene films, (c) C, O, and N for CNT:PANI film.

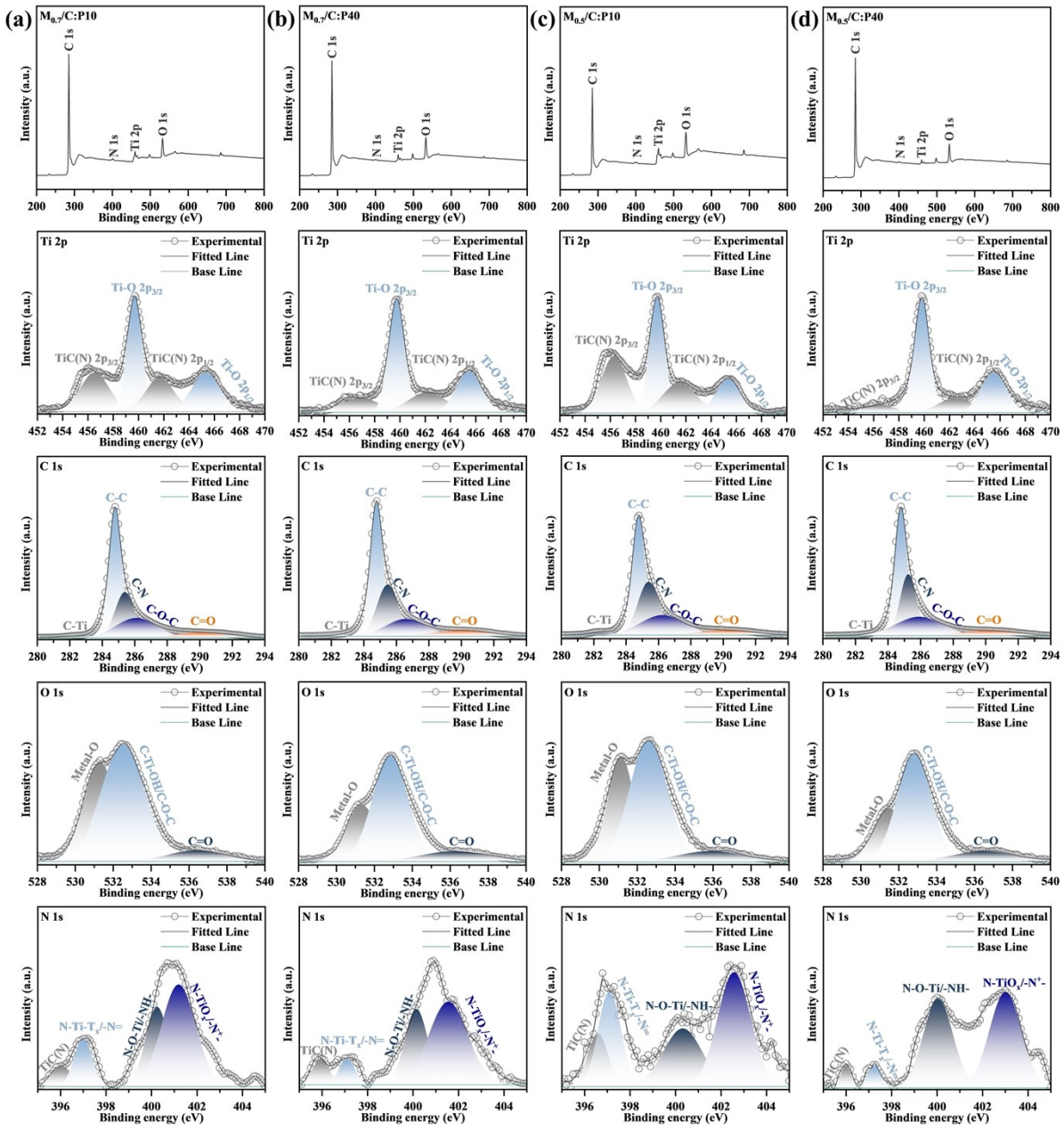

Fig. S7 XPS spectra of full range spectrum and high-resolution energy spectra (Ti, C, O, N) of (a) $M_{0.7}$/C:P10, (b) $M_{0.7}$/C:P40, (c) $M_{0.5}$/C:P10, and (d) $M_{0.5}$/C:P40 composite films.

Table. S2 The XPS peak fitting and assignment of the $Ti_3(C_{1-y}N_y)_2T_x$ $(y = 0.3, 0.5)$ MXenes films and C:P film.

	BE (eV)

Region	$Ti_3(C_{0.7}N_{0.3})_2T_x$	Assigned to	Region	$Ti_3(C_{0.5}N_{0.5})_2T_x$	Assigned to	Region	C:P	Assigned to	Ref.
Ti	456.0 (461.4)	TiC(N)	**Ti $2p_{3/2}$**	456.1 (461.3)	TiC(N)		-	-	[4]
$2p_{3/2}$	459.2 (464.4)	Ti-O	**($2p_{1/2}$)**	458.8 (464.1)	Ti-O		-	-	[4]
($2p_{1/2}$)									
	282.1	TiC(N)		281.7	TiC(N)		284.9	C-C	[4]
C 1s	284.8	C-C	**C 1s**	284.8	C-C	**C 1s**	285.3	C-N	[4]
	285.6	C-O-C		285.6	C-O-C		286.0	C-O-C	[4]
	288.7	C=O		288.7	C=O		290.2	C=O	[4]
	530.3	Metal-O		530.1	Metal-O		533.0	C-O-C	[4]
O 1s	532.2	C-Ti-OH_x	**O 1s**	531.6	C-Ti-OH_x	**O 1s**	534.1	C-O	[4]
							537.1	C=O	[4]
	396.4	TiC(N)		395.8	TiC(N)		396.8	-N=	[4]
N 1s	397.1	N-Ti-T_x	**N 1s**	396.6	N-Ti-T_x	**N 1s**	400.0	-NH-	[5]
	400.1	N-O-Ti		399.3	N-O-Ti		402.7	$-N^+-$	[5, 6]
	401.9	N-TiO_x		401.7	N-TiO_x				

Table. S3 The XPS peak fitting and assignment of the M_X/C:P composite films.

	BE (eV)							
Region	**$M_{0.7}$/C:P10**	**$M_{0.7}$/C:P20**	**$M_{0.7}$/C:P40**	**$M_{0.5}$/C:P10**	**$M_{0.5}$/C:P20**	**$M_{0.5}$/C:P40**	**Assigned to**	**Ref.**
Ti $2p_{3/2}$	456.8 (462.2)	456.7 (461.9)	456.5 (461.6)	456.6 (462.5)	457.1 (462.6)	456.5 (461.6)	TiC(N)	[4]
($2p_{1/2}$)	459.7 (465.4)	459.4 (465.2)	459.5 (465.4)	459.8 (465.5)	459.7 (465.5)	459.6 (465.4)	Ti-O	[4]
	282.4	282.5	282.7	282.9	283.4	282.4	TiC(N)	[4]
C 1s	284.7	284.7	284.7	284.8	284.7	284.8	C-C	[4]
	285.5	285.3	285.4	285.3	285.3	285.4	C-N	[4]
	286.6	286.4	286.1	285.9	285.9	286.3	C-O-C	[4]
	290.2	290.4	290.2	290.2	290.4	290.3	C=O	[4]
	531.3	531.1	531.3	531.5	531.2	531.1	Metal-O	[4]
O 1s	532.8	532.7	532.5	532.8	532.5	532.6	C-Ti-OH/C-O-C	[4]
	536.3	536.5	536.6	536.5	536.5	536.2	C=O	[4]
	395.9	396.6	396.2	396.0	396.4	396.5	TiC(N)	[4]
N 1s	397.1	397.0	397.0	397.2	396.9	397.1	N-Ti-T_X/-N=	[4]
	400.2	400.4	400.3	400.0	400.8	400.3	N-O-Ti/-NH-	[5]
	401.5	401.4	401.2	402.9	402.4	402.6	N-TiO_x/$-N^+-$	[5, 6]

High-resolution XPS analyses of (Fig. S7) were conducted for Ti 2p, C 1s, O 1s, and N 1s regions to further elucidate the bonding environments in the M_X/C:P composite films. The

Ti 2p spectra reveal peaks corresponding to TiC(N) and Ti–O bonds, while the C 1s spectra exhibit features associated with TiC(N), C–C, C–N, C–O–C, and C=O groups. The O 1s region identifies the presence of Metal–O and C–Ti–OH or C-O-C and C=O species. Distinct N 1s peaks in the M_x/C:P20 composite films are assigned to TiC(N), N–Ti–T_x/–N= (quinoid amine), N–O–Ti/–NH– (benzenoid amine), and N–TiO_x/–N^+– (iminium species) [4-7].

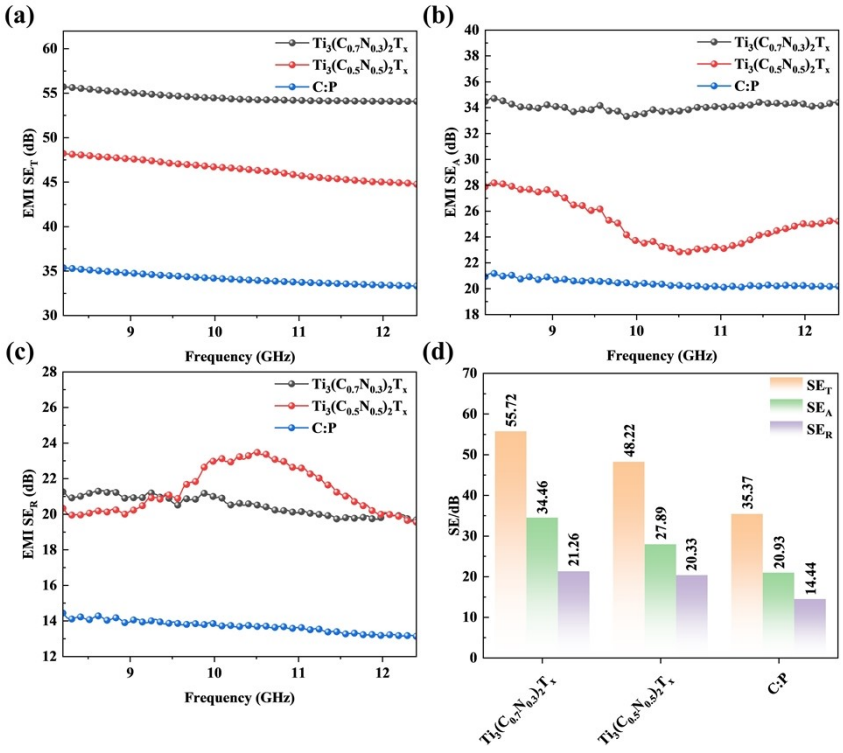

Fig. S8 EMI properties of $Ti_3(C_{0.7}N_{0.3})_2T_x$, $Ti_3(C_{0.5}N_{0.5})_2T_x$ MXenes, and C:P films in the frequency range of 8.2–12.4 GHz: (a) SE_T, (b) SE_R, (c) SE_A, and (d) the comparison among SE_T, SE_R, and SE_A.

(Figs. S8a–d) show the EMI performance of the $Ti_3(C_{0.7}N_{0.3})_2T_x$, $Ti_3(C_{0.5}N_{0.5})_2T_x$ MXenes and C:P films in terms of SE_T, SE_A, and SE_R within the X-band frequency range of 8.2–12.4

GHz.[8] The SE_T values of $Ti_3(C_{0.7}N_{0.3})_2T_x$ (55.72 dB), $Ti_3(C_{0.5}N_{0.5})_2T_x$ (48.22 dB), and C:P films (35.37 dB) exceed the minimum SE_T requirement of 20 dB for commercial EMI shielding materials, corresponding to 99.99% attenuation of incident electromagnetic waves.[9-11] $Ti_3(C_{0.7}N_{0.3})_2T_x$ MXene exhibits the highest SE_A and SE_R compared to $Ti_3(C_{0.5}N_{0.5})_2T_x$ MXene and the C:P films. This indicates that absorption plays a more significant role in the total shielding effectiveness of $Ti_3(C_{0.7}N_{0.3})_2T_x$ films compared with $Ti_3(C_{0.5}N_{0.5})_2T_x$ MXene, CNT:PANI, and their composite films.

Table. S4 Summarizes the EMI shielding performance of MXenes and their composites.

Compositions	MXene filler (wt%) @Methods	Density (g cm^{-3})	Thickness (µm)	Conductivity σ (S m^{-1})	EMI SE (dB)	SSE/t (dB cm^2 g^{-1})	Ref.
$Ti_3C_2T_x$	100@VAF	2.39	45.0	480000	92.0	-	10
Ti_3CNT_x	100@VAF	-	40.0	112500	61.4	-	9
$Ti_3C_2T_x$	100@VAF	2.70	5.0	857000	57.4	-	11
Ti_3CNT_x	100@VAF	-	5.0	271200	49.7	-	11
$Ti_3C_2T_x$	100@VAF	2.33	5.0	432000	56.1	48154.51	12
Ti_3C_2/Graphene	-@SA	0.41	15.0	100081	47.0	-	13
rGO/SWCNTs/PDMS	0.28@BF	-	200.0	120.0	31.0	110.70	14
$Ti_3C_2T_x$/PANI	70@VAF	-	40.0	2440	36.0	-	15
$Ti_3C_2T_x$/Ni/PVDF	10@SCM	1.65	100.0	-	19.5	1177	16
Ti_3CNT_x@/Ni@C	95@VAF	-	10.0	190000	40.0	-	17
Ti_3C_2/PEDOT: PSS	70@VAF	1.94	11.1	34050	42.10	19497.8	18
Ti_3C_2/PANI/CNTs	76@VAF	-	10.0	43000	49.8	-	19
$Ti_3C_2T_x$/cellulose/CNT	-@VAF	1.26	38.0	2500.10	38.4	8020.0	20
PANI/MXene/CF	-@LBL	-	55.0	24.57	26.0	135.5	21
MXene/CNF-PPy	-@VAF	-	5.0	2050.0	45.8	-	22
Ti_3C_2/PANI/Carbon	-@LBL	-	-	142	21.0	-	23
PAN@PPy/Ti_3C_2	46.78@VDP	-	55	2250	32	17534.50	24
$Ti_3(C_{0.7}N_{0.3})_2T_x$	100@VAF	2.79	5.0	293799.30	55.72	39942.65	This work
$Ti_3(C_{0.5}N_{0.5})_2T_x$	100@VAF	2.43	5.0	233495.40	48.22	39687.24	This work
C:P	70:30@VAF	1.06	13.0	26112.80	35.37	25667.63	This work
$M_{0.7}$/C:P20	80@VAF	2.03	9.0	76087.26	45.03	33281.59	This work
$M_{0.5}$/C:P20	80@VAF	1.85	10.0	64707.66	41.93	29362.74	This work

PANI, polyaniline; rGO, reduced graphene oxide; PDMS, Polydimethylsiloxane; Ni, Nickle; PVDF, Polyvinylidene fluoride; C, Carbon; PEDOT, poly(3,4-ethylenedioxythiophene); PSS, polystyrene sulfonate; C:P, MWCNTs:PANI; VAF, vacuum assisted filtration; BF, backfilling; SA, self-assembly; SCM, solution casting method, SSLBL, spin spray layer-by-layer; LBL, layer-by-layer; VDP, vapor deposition process.

References

1. T. Zhang, C. E. Shuck, K. Shevchuk, M. Anayee and Y. Gogotsi, *J. Am. Chem. Soc*., 2023, 145, 22374-22383.

2. S. Kim, M. W. Jeong, K. Kim, U. g. Kim, M. Kim, S. Y. Lee and Y. C. Joo, *RSC Adv*., 2023, 13, 2131-2139.

3. J. Swapnalin, B. Koneru, R. Pothu, P. Banerjee, R. Boddula, A. B. Radwan and N. Al-Qahtani, *Appl. Phys. Lett*., 2023, 122.

4. J. Halim, K. M. Cook, M. Naguib, P. Eklund, Y. Gogotsi, J. Rosen and M. W. Barsoum, *Appl. Surf. Sci*., 2016, 362, 406-417.

5. L. Ding, Q. Li, D. Zhou, H. Cui, R. Tang and J. Zhai, *Electrochim. Acta*, 2012, 77, 302-308.

6. J. Yang, H. Bai, X. Tan and J. Lian, *Appl. Surf. Sci*., 2006, 253, 1988-1994.

7. K. Donthula, U. R. Malothu, R. Araga, R. Vooradi, V. S. Patnaikuni, M. Reddy and M. Kakunuri, *Polym. Compos*., 2023, 44, 7571-7584.

8. L. Gao, C. Li, W. Huang, S. Mei, H. Lin, Q. Ou, Y. Zhang, J. Guo, F. Zhang and S. Xu, *Chem. Mater*., 2020, 32, 1703-1747.

9. A. Iqbal, F. Shahzad, K. Hantanasirisakul, M. K. Kim, J. Kwon, J. Hong, H. Kim, D. Kim, Y. Gogotsi and C. M. Koo, *Science*, 2020, 369, 446-450.

10. F. Shahzad, M. Alhabeb, C. B. Hatter, B. Anasori, S. Man Hong, C. M. Koo and Y.

Gogotsi, *Science*, 2016, 353, 1137-1140.

11. M. Han, C. E. Shuck, R. Rakhmanov, D. Parchment, B. Anasori, C. M. Koo, G. Friedman and Y. Gogotsi, *ACS Nano*, 2020, 14, 5008-5016.

12. M. I. Jahanger, S. A. Soomro, M. U. Khan, Y. Bao, M. Jiang, L. Chu, Q. Feng and C. Hu, *Appl. Surf. Sci*., 2025, 692, 162705.

13. X. Tang, J. Luo, Z. Hu, S. Lu, X. Liu, S. Li, X. Zhao, Z. Zhang, Q. Lan and P. Ma, *Nano Res*., 2023, 16, 1755-1763.

14. S. Zhao, Y. Yan, A. Gao, S. Zhao, J. Cui and G. Zhang, *ACS Appl. Mater. Interfaces*, 2018, 10, 26723-26732.

15. Y. Zhang, L. Wang, J. Zhang, P. Song, Z. Xiao, C. Liang, H. Qiu, J. Kong and J. Gu, *Compos. Sci. Technol*., 2019, 183, 107833.

16. S. J. Wang, D. S. Li and L. Jiang, *Adv. Mater. Interfaces*, 2019, 6, 1900961.

17. Z. Xiang, X. Wang, X. Zhang, Y. Shi, L. Cai, X. Zhu, Y. Dong and W. Lu, *Carbon*, 2022, 189, 305-318.

18. R. Liu, M. Miao, Y. Li, J. Zhang, S. Cao and X. Feng, *ACS Appl. Mater. Interfaces*, 2018, 10, 44787-44795.

19. Y. S. Fang, P. He, Y. Z. Cai, W. Q. Cao and M. S. Cao, *Ceram. Int*., 2021, 47, 25531-25540.

20. W. Cao, C. Ma, S. Tan, M. Ma, P. Wan and F. Chen, *Nano-Micro Lett*., 2019, 11, 72.

21. G. Yin, Y. Wang, W. Wang and D. Yu, *Colloids Surf. A Physicochem. Eng. Asp*., 2020, 601, 125047.

22. H. Chai, J. Tie, Y. Zhong, L. Zhang, X. Feng, H. Xu and Z. Mao, *Cellulose*, 2024, 31, 6435-6452.

23. Y. Mao, D. Wang and S. Fu, *Compos. Part A Appl. Sci. Manuf.*, 2022, 153, 106751.

24. F. Wu, Z. Tian, P. Hu, J. Tang, X. Xu, L. Pan, J. Liu, P. Zhang and Z. Sun, *Nanoscale*, 2022, 14, 18133-18142.